Impaired excitability of somatostatin- and parvalbumin-expressing cortical interneurons in a mouse model of Dravet syndrome

Chao Tai[a], Yasuyuki Abe[a,b], Ruth E. Westenbroek[a], Todd Scheuer[a], and William A. Catterall[a,1]

[a]Department of Pharmacology, University of Washington, Seattle, WA 98195; and [b]Medicinal Safety Research Laboratories, Daiichi Sankyo Co., Ltd., Tokyo 134-8630, Japan

Contributed by William A. Catterall, June 17, 2014 (sent for review May 6, 2014)

Haploinsufficiency of the voltage-gated sodium channel $Na_V1.1$ causes Dravet syndrome, an intractable developmental epilepsy syndrome with seizure onset in the first year of life. Specific heterozygous deletion of $Na_V1.1$ in forebrain GABAergic-inhibitory neurons is sufficient to cause all the manifestations of Dravet syndrome in mice, but the physiological roles of specific subtypes of GABAergic interneurons in the cerebral cortex in this disease are unknown. Voltage-clamp studies of dissociated interneurons from cerebral cortex did not detect a significant effect of the Dravet syndrome mutation on sodium currents in cell bodies. However, current-clamp recordings of intact interneurons in layer V of neocortical slices from mice with haploinsufficiency in the gene encoding the $Na_V1.1$ sodium channel, *Scn1a*, revealed substantial reduction of excitability in fast-spiking, parvalbumin-expressing interneurons and somatostatin-expressing interneurons. The threshold and rheobase for action potential generation were increased, the frequency of action potentials within trains was decreased, and action-potential firing within trains failed more frequently. Furthermore, the deficit in excitability of somatostatin-expressing interneurons caused significant reduction in frequency-dependent disynaptic inhibition between neighboring layer V pyramidal neurons mediated by somatostatin-expressing Martinotti cells, which would lead to substantial disinhibition of the output of cortical circuits. In contrast to these deficits in interneurons, pyramidal cells showed no differences in excitability. These results reveal that the two major subtypes of interneurons in layer V of the neocortex, parvalbumin-expressing and somatostatin-expressing, both have impaired excitability, resulting in disinhibition of the cortical network. These major functional deficits are likely to contribute synergistically to the pathophysiology of Dravet syndrome.

Dravet syndrome (DS), also referred to as "severe myoclonic epilepsy in infancy," is a rare genetic epileptic encephalopathy characterized by frequent intractable seizures, severe cognitive deficits, and premature death (1–3). DS is caused by loss-of-function mutations in *SCN1A*, the gene encoding type I voltage-gated sodium channel $Na_V1.1$, which usually arise de novo in the affected individuals (4–7). Like DS patients, mice with heterozygous loss-of-function mutations in *Scn1a* exhibit ataxia, sleep disorder, cognitive deficit, autistic-like behavior, and premature death (8–14). Like DS patients, DS mice first become susceptible to seizures caused by elevation of body temperature and subsequently experience spontaneous myoclonic and generalized tonic-clonic seizures (11). Global deletion of $Na_V1.1$ impairs Na^+ currents and action potential (AP) firing in GABAergic-inhibitory interneurons (8–10), and specific deletion of $Na_V1.1$ in forebrain interneurons is sufficient to cause DS in mice (13, 15). These data suggest that the loss of interneuron excitability and resulting disinhibition of neural circuits cause DS, but the functional role of different subtypes of interneurons in the cerebral cortex in DS remains unknown.

Neocortical GABAergic interneurons shape cortical output and display great diversity in morphology and function (16, 17). The expression of parvalbumin (PV) and somatostatin (SST) defines two large, nonoverlapping groups of interneurons (16, 18, 19). In layer V of the cerebral cortex, PV-expressing fast-spiking interneurons and SST-expressing Martinotti cells each account for ∼40% of interneurons, and these interneurons are the major inhibitory regulators of cortical network activity (17, 20). Layer V PV interneurons make synapses on the soma and proximal dendrites of pyramidal neurons (18, 19), where they mediate fast and powerful inhibition (21, 22). Selective heterozygous deletion of *Scn1a* in neocortical PV interneurons increases susceptibility to chemically induced seizures (23), spontaneous seizures, and premature death (24), indicating that this cell type may contribute to *Scn1a* deficits. However, selective deletion of *Scn1a* in neocortical PV interneurons failed to reproduce the effects of DS fully, suggesting the involvement of other subtypes of interneurons in this disease (23, 24). Layer V Martinotti cells have ascending axons that arborize in layer I and spread horizontally to neighboring cortical columns, making synapses on apical dendrites of pyramidal neurons (17, 25, 26). They generate frequency-dependent disynaptic inhibition (FDDI) that dampens excitability of neighboring layer V pyramidal cells (27–29), contributing to maintenance of the balance of excitation and inhibition in the neocortex. However, the functional roles of Martinotti cells and FDDI in DS are unknown.

Because layer V forms the principal output pathway of the neocortex, reduction in inhibitory input to layer V pyramidal cells would have major functional consequences by increasing excitatory output from all cortical circuits. However, the effects of the DS mutation on interneurons and neural circuits that provide inhibitory input to layer V pyramidal cells have not been determined. Here we show that the intrinsic excitability of layer V fast-spiking PV interneurons and SST Martinotti cells and the

Significance

Dravet syndrome (DS) is an intractable childhood epilepsy syndrome accompanied by mental disability, behaviors similar to autism, and premature death. DS is caused by dominant loss-of-function mutations in the gene encoding the $Na_V1.1$ sodium channel, *SCN1A*, which initiates electrical signals in the nerve cells of the brain. The physiological basis for this disease is largely unknown. Here we describe the functional effects of DS mutations on inhibitory neurons in the cerebral cortex in mice. Our results show that two major types of inhibitory neurons are impaired in generation of electrical signals by a DS mutation, whereas excitatory neurons are unaffected. The resulting imbalance of excitatory over inhibitory electrical signaling would contribute in an important way to the symptoms of DS.

Author contributions: C.T., Y.A., R.E.W., T.S., and W.A.C. designed research; C.T., Y.A., and R.E.W. performed research; C.T., Y.A., R.E.W., and T.S. analyzed data; and C.T., R.E.W., T.S., and W.A.C. wrote the paper.

The authors declare no conflict of interest.

[1]To whom correspondence should be addressed. Email: wcatt@uw.edu.

This article contains supporting information online at www.pnas.org/lookup/suppl/doi:10.1073/pnas.1411131111/-/DCSupplemental.

FDDI mediated by Martinotti cells are reduced dramatically in DS mice, leading to an imbalance in the excitation/inhibition ratio. Our results suggest that loss of $Na_V1.1$ in these two major types of interneurons may contribute synergistically to increased cortical excitability, epileptogenesis, and cognitive deficits in DS.

Results

Sodium Currents in Cell Bodies of Cortical GABAergic-Inhibitory Interneurons. We first studied sodium currents in dissociated interneurons from the cerebral cortex of WT and $Na_V1.1$ heterozygous (HET) mice at postnatal day (P) 14 and P21 (Fig. S1) using methods previously developed for hippocampal interneurons (8, 10). Surprisingly, although we found a trend toward a decrease in peak sodium currents in the cell bodies of homozygous $Na_V1.1$-knockout mice at P14, it did not reach significance (Fig. S1 *B*, *D*, and *E*). We also observed an insignificant decrease in peak sodium currents and no change in voltage dependence of activation for mean sodium currents in the cell bodies of dissociated cortical interneurons from HET mice at P14 (Fig. S1 *B*, *D*, and *E*) and P21 (Fig. S1 *C*, *F*, and *G*). In contrast, previous studies have revealed decreased sodium current in dissociated interneurons from *Scn1a* HETs in hippocampus (8) and cerebellum (10). These results suggested that the excitability is less impaired in the cell bodies of cortical interneurons than in the interneurons in these other brain areas. However, dissociated interneurons lose their dendritic and axonal components, which may obscure significant functional deficits in excitability. For example, $Na_V1.1$ and other sodium channels are expressed at high levels in axon initial segments of interneurons, which are not retained in dissociated neurons. Therefore, to examine the excitability of neocortical interneurons and the basis for cortical hyperexcitability in DS further, we studied intact neurons in brain slices in current-clamp mode, focusing on PV and SST interneurons in layer V of the neocortex.

Reduced Excitability of Layer V PV Interneurons. $Na_V1.1$ channels are localized in both cell somata and axon initial segments of cortical PV interneurons (8, 9, 30, 31), as confirmed in this study (Fig. 1*A*). Although several studies have suggested an important role for PV interneurons in DS (9, 23, 24), the physiological consequences of DS mutations in these neurons have not been analyzed extensively in previous work. We examined the electrophysiological properties of layer V PV interneurons in $Na_V1.1$ HET and WT mice that had been crossed with the G42 PV reporter strain. PV interneurons were identified by eGFP fluorescence in acute brain slices from P21 mice as described in *Materials and Methods*. Whole-cell patch-clamp recordings showed that WT and HET PV interneurons have indistinguishable input resistance, membrane capacitance, and resting membrane potential (Table 1). In current-clamp recordings, WT PV interneurons displayed typical, sustained high-frequency trains of brief APs with little spike frequency adaptation in response to incremental current injections (3 s) (Fig. 1*B*). HET PV interneurons displayed AP patterns similar to those in WT PV interneurons but fired fewer APs (Fig. 1 *B* and *C*) at lower frequencies (Fig. 1 *B* and *D*) in response to the same depolarizing current injection. The rheobase (the smallest current injection that triggered an AP) also was increased (Fig. 1*H*). We compared adaptation of the amplitude or frequency of APs in WT and HET PV interneurons during the first 100 APs in response to the minimal current step that triggered a train of at least 100 APs but did not observe significant changes (Table 1). We also measured the single AP properties of PV interneurons. Both WT and HET PV interneurons fired typical brief APs with a large, rapid afterhyperpolarization (Fig. 1*E*), but HET PV interneurons displayed a significantly increased AP threshold (Fig. 1*F*) and reduced spike amplitude (Fig. 1*G*). AP width was not significantly changed (Fig. 1*I*). These data show that deletion of $Na_V1.1$ channels substantially reduced the excitability of cortical layer V PV interneurons in HET animals as reflected in both single AP properties and AP firing pattern.

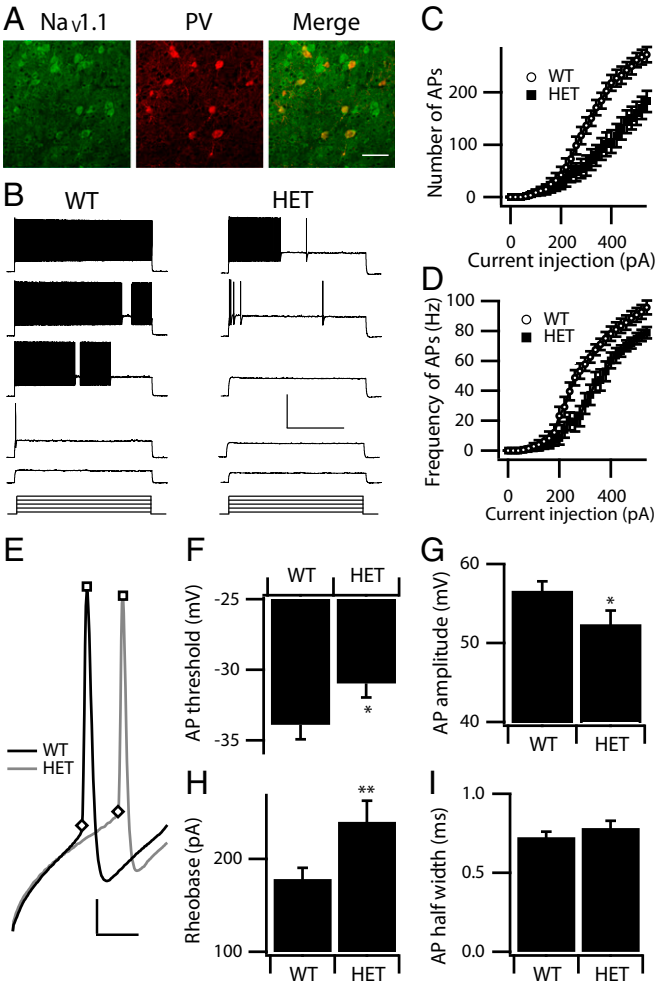

Fig. 1. Excitability of cortical layer V PV interneurons. (*A*) Double labeling of cortical layer V PV interneurons from WT animals labeled with anti-$Na_V1.1$ antibody (green) and anti-PV antibody (red). The merged image shows double-labeled PV interneurons in yellow to illustrate the presence of $Na_V1.1$ channels in PV interneurons in cortical layer V. (Scale bar: 100 μm.) (*B*) Sample whole-cell current-clamp recordings in response to incremental steps of current (3 s, ranging from 140–380 pA), in a WT and a HET PV interneuron. (Calibration: 1 s, 40 mV.) (*C* and *D*) The mean number (*C*) and frequency (*D*) of APs in response to each step for WT ($n = 19$) and HET ($n = 18$). (*E–I*) Properties of individual WT and HET APs. (*E*) Expanded and superimposed individual APs from the recordings of WT and HET PV interneurons in *B*. (Calibration: 2 ms, 15 mV.) (*F*) Mean AP threshold. (*G*) Mean AP amplitude. (*H*) Mean rheobase. (*I*) Mean AP half width. Significant differences between WT and HET are expressed as $*P < 0.05$; $**P < 0.01$.

We examined the reliability of AP firing in PV interneurons in response to a train of 100 brief rectangular current injections (10 ms) at 1, 2, 5, 10, 20, and 50 Hz. The current amplitude was set at the minimal level required to trigger a single AP. As in 3-s recordings, the rheobase for firing APs in PV interneurons was increased for HET cells (WT: 356.8 ± 30.6 pA; HET: 464.4 ± 42.3 pA; $P < 0.05$) (Fig. 2*A*). Both WT and HET PV interneurons generate APs with a very low failure rate at 1 Hz and 2 Hz (Fig. 2*C*); however, HET PV interneurons showed increased AP failure rate compared with WT at higher stimulation frequencies (5–50 Hz) (Fig. 2 *B* and *C*). These results indicate that the loss of $Na_V1.1$ channels reduces the reliability of spike firing at higher stimulation frequencies in HET animals and support the

Table 1. Electrophysiological parameters of pyramidal neurons and interneurons in neocortex

	PV interneurons		SST interneurons		Pyramidal neurons	
	WT (n = 19)	HET (n = 18)	WT (n = 21)	HET (n = 23)	WT (n = 35)	HET (n = 35)
V_{rest}, mV	−65.5 ± 0.7	−65.1 ± 0.7	−73.2 ± 1.0	−73.5 ± 0.4	−58.2 ± 0.6	−59.1 ± 0.6
R_{in}, MΩ	174.1 ± 14.8	172.7 ± 18.4	326.9 ± 29.6	312.9 ± 15.0	260.0 ± 20.4	251.0 ± 13.2
C_m, pF	29.2 ± 1.0	30.8 ± 1.7	24.8 ± 1.3	25.4 ± 1.6	39.2 ± 1.8	40.8 ± 1.9
Rheobase, pA	178.4 ± 12.0	241.1 ± 22.0**	51.9 ± 6.6	82.6 ± 4.7***	98.6 ± 5.5	94.3 ± 4.9
Threshold, mV	−33.9 ± 1.0	−30.9 ± 1.0*	−38.3 ± 1.0	−35.5 ± 0.7*	−32.1 ± 1.0	−31.7 ± 0.9
Amplitude, mV	56.1 ± 1.4	52.4 ± 1.7*	86.5 ± 1.7	87.1 ± 1.1	81.8 ± 0.9	82.6 ± 1.1
AP half width, ms	0.72 ± 0.03	0.78 ± 0.05	1.49 ± 0.08	1.43 ± 0.06	2.1 ± 0.09	1.9 ± 0.09
Frequency#, Hz	57.8 ± 4.5	31.5 ± 6.5***	40.9 ± 3.8	29.7 ± 2.5***	14.2 ± 1.5	15.6 ± 1.1
AP amplitude adaptation ratio	0.90 ± 0.03	0.91 ± 0.02	1.01 ± 0.03	1.02 ± 0.03	0.92 ± 0.04	0.94 ± 0.04
AP frequency adaptation ratio	0.75 ± 0.02	0.74 ± 0.02	0.36 ± 0.03	0.38 ± 0.02	0.85 ± 0.03	0.86 ± 0.04

For an explanation of the parameters, see *Materials and Methods*. Values shown are expressed as mean ± SEM. Significant differences between WT and HET are expressed as $*P < 0.05$; $**P < 0.01$; $***P < 0.001$, two-sample Student t test.
#Frequencies for PV interneurons were measured at 300-pA current injection (3 s), and frequencies for SST interneurons, and pyramidal neurons were measured at 200-pA current injection (1 s).

conclusion that $Na_V1.1$ channels are required for PV interneurons to fire with high precision and fidelity in response to repetitive inputs.

Impaired Monosynaptic Transmission Between Layer V Pyramidal Neurons and PV Neurons. To analyze how the reduced excitability of PV interneurons affects their response to excitatory synaptic input from pyramidal neurons, we performed dual current-clamp recordings on pairs of neighboring pyramidal neurons and PV neurons in layer V (Fig. 3*A*). Stimulation of the pyramidal (PY) neuron to generate a single AP (Pre PY) elicited a postsynaptic response (Post PV) (Fig. 3*B*). Mean amplitudes of excitatory postsynaptic potentials (EPSPs) in PV neurons were only 53% as large in HET cells as in WT (Fig. 3*C*). These data from DS mice illustrate the impact of the reduced excitability of postsynaptic PV neurons observed in the experiments of Figs. 1 and 2 on their response to excitatory synaptic input from layer V pyramidal neurons.

We also examined the inhibitory monosynaptic connection from layer V PV neurons to pyramidal neurons (Fig. 3 *D* and *E*). Stimulation of PV neurons to generate trains of 1–20 presynaptic APs at 70 Hz reliably elicited postsynaptic responses whose size increased with AP number (Fig. 3*E*) but did not change between WT and HET (Fig. 3*D*). Thus, the ability of layer V pyramidal neurons to respond to inhibitory synaptic input from PV neurons was not impaired when PV neurons were stimulated strongly enough to generate the same number of presynaptic APs in PV neurons from WT and DS mice. These results are consistent with impaired excitability of PV neurons but not of layer V pyramidal neurons in DS mice.

Reduced Excitability of Layer V Martinotti Cells. We next studied layer V SST-expressing Martinotti cells. Immunohistochemistry experiments showed that $Na_V1.1$ channels are expressed in layer V SST interneurons (Fig. 4*A*). However, the physiological effect of deletion of these channels in SST interneurons in DS has not been studied. We identified Martinotti cells, as described in *Materials and Methods*. WT and HET Martinotti cells had indistinguishable input resistance, membrane capacitance, and resting membrane potential (Table 1). In current-clamp recordings, WT Martinotti cells displayed a low discharge rate and typical AP frequency accommodation in response to incremental steps of current injection (1 s), as previously reported (27, 28, 32, 33) (Fig. 4*B*). HET Martinotti cells generated AP patterns similar to those in the WT cells but fired fewer APs (Fig. 4 *B* and *C*) at lower frequencies (Fig. 4 *B* and *D*) in response to equal injections of depolarizing current, and the rheobase for inhibiting AP trains in HET cells was higher in HET than in WT Martinotti cells (Fig. 4*G*). WT and HET Martinotti cells displayed similar strong adaptation of AP amplitude and frequency in response to trains of stimuli (Table 1). In analysis of single AP properties, we found that HET Martinotti cells have a significantly higher spike threshold (Fig. 4*F*), but spike amplitude (Fig. 4*H*) and width (Fig. 4*I*) did not change significantly. These results show that deletion of $Na_V1.1$ channels dramatically reduces the likelihood that Martinotti cells in cortical layer V of HET animals will fire in response to a wide range of input stimuli.

Interneurons must fire repetitive APs to counter the excitation of pyramidal neurons in cortical circuits effectively. We examined the reliability of AP firing in Martinotti cells in response to a train of 100 brief, rectangular current injections (10 ms) at 1, 2, 5, 10, and 20 Hz with the current amplitude set at the minimal level required to trigger a single AP. Both WT and HET Martinotti cells generate APs with low failure rate at 1 Hz and 2 Hz (Fig. 5 *A*

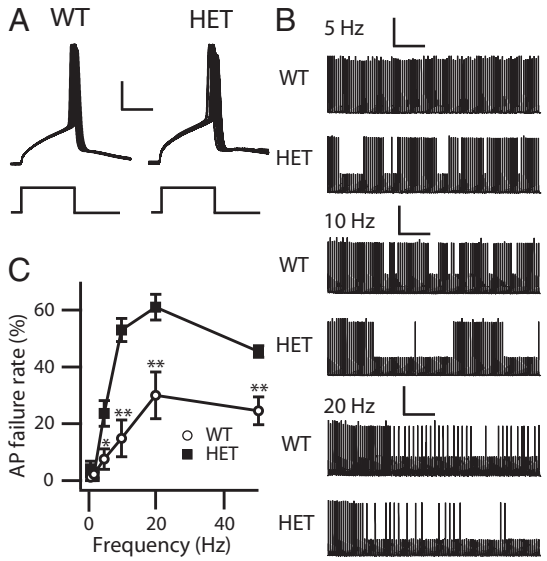

Fig. 2. Ability of cortical layer V PV interneurons to sustain repetitive firing. Whole-cell current-clamp recordings in response to trains of 100 10-ms pulses. Pulse amplitude was the minimum current required to trigger an AP. Frequency was 1, 2, 5, 10, 20, or 50 Hz. (*A*) Sample APs of the 1-Hz train for WT and HET PV interneurons. (Calibration: 5 ms, 20 mV.) (*B*) Sample traces at 5 (calibration: 2 s, 25 mV), 10 (calibration: 1 s, 25 mV), and 20 (calibration: 0.5 s, 25 mV) Hz. (*C*) Percent of stimuli that failed to produce an AP as a function of frequency. $*P < 0.05$; $**P < 0.01$.

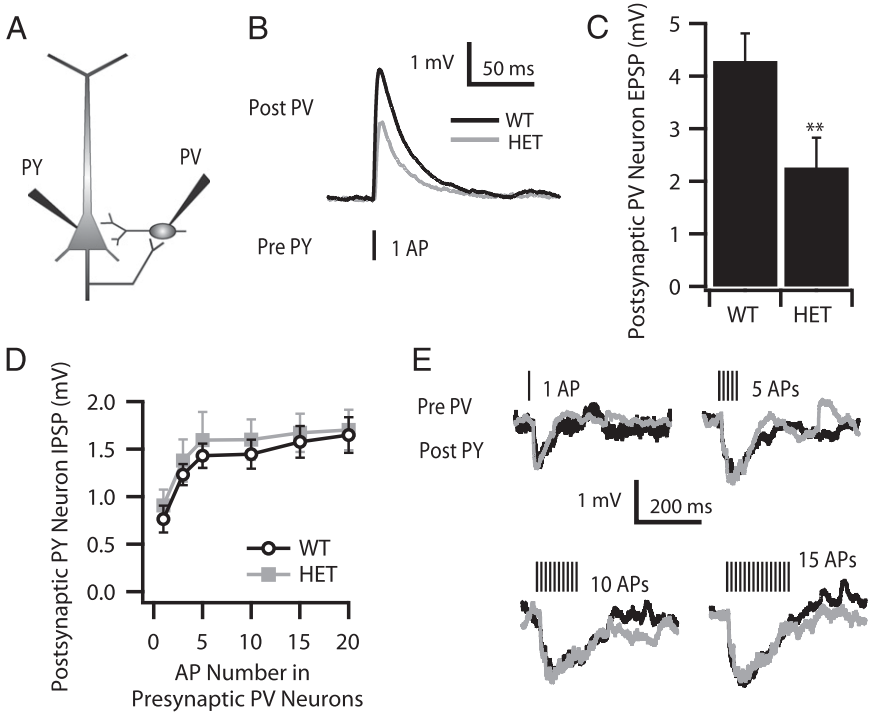

Fig. 3. Monosynaptic connection between layer V pyramidal neurons and fast-spiking PV interneurons. (*A*) Cartoon showing the dual patch clamp of a layer V pyramidal neuron (PY) and a neighboring layer V PV interneuron. (*B* and *C*) Excitatory monosynaptic connection from layer V pyramidal neurons to PV interneurons. (*B*) Sample traces (black for WT, gray for HET) of evoked EPSPs in postsynaptic PV interneurons (Post PV) in response to a single AP in a presynaptic pyramidal neuron (Pre PY). (*C*) The amplitudes of postsynaptic EPSPs in PV interneurons were reduced significantly in HET ($n = 8$) compared with WT ($n = 10$) (4.29 ± 0.52 mV in WT vs. 2.26 ± 0.57 mV in HET; $^{**}P = 0.009$) in response to APs in presynaptic pyramidal neurons. (*D* and *E*) Inhibitory monosynaptic connection from layer V PV interneurons to pyramidal neurons. (*D*) The amplitudes of inhibitory postsynaptic potentials (IPSPs) in layer V pyramidal neurons as a function of number of presynaptic APs in PV interneurons (WT: $n = 7$; HET: $n = 7$). (*E*) Sample traces (black for WT, gray for HET) of postsynaptic IPSP in layer V pyramidal neurons in response to different numbers of APs in presynaptic PV interneurons.

and *C*). However, the failure rate increased markedly in HET Martinotti cells at stimulation frequencies of 5–20 Hz (Fig. 5 *B* and *C*), a frequency range that is crucial for neocortical function (34, 35). These results indicate that the loss of $Na_V1.1$ channels reduces the reliability of Martinotti cells to fire repetitively at physiologically relevant stimulus frequencies.

Reduced Disynaptic Inhibition Mediated by Martinotti Cells in Layer V. Excitatory inputs onto layer V Martinotti cells are strongly facilitating, and high-frequency repetitive spiking (~70 Hz) in a single layer V pyramidal neuron can drive a nearby Martinotti cell to fire and provide feedback inhibition to neighboring layer V pyramidal neurons across layers and columns. FDDI between layer V pyramidal neurons is an important activity-dependent synaptic pathway controlling circuit dynamics in all neocortical areas (27, 28, 36). To test whether loss of $Na_V1.1$ channels results in reduced disynaptic inhibition, we studied FDDI mediated by Martinotti cells in WT and HET mice. We performed dual current-clamp recordings on neighboring thick-tufted layer V pyramidal neurons (somatic distance less than 100 μm) in acute neocortical slices (Fig. 6*A*). When pyramidal neurons were stimulated with trains of APs (15 pulses at 70 Hz), we observed inhibitory responses on neighboring pyramidal neurons in both WT and HET animals as a consequence of FDDI (Fig. 6*B*). Consistent with previous reports (27, 28, 36), this inhibition could be blocked completely by bath perfusion of 10 μM 6-cyano-7-nitroquinoxaline-2,3-dione, an AMPA-receptor antagonist, confirming the requirement for excitatory synaptic transmission (Fig. S2 *A* and *B*). Bath application of bicuculline (10 μM), a $GABA_A$-receptor antagonist, also completely blocked FDDI, confirming that disynaptic transmission was mediated by GABAergic Martinotti cells (Fig. S2 *C* and *D*). The probability of observing measurable FDDI between neighboring pyramidal neurons when testing with 15 pulses at 70 Hz was reduced significantly in HET animals (WT: 48%; HET: 26%; Fisher's exact test, $P < 0.01$) (Fig. 6*C*). Among the successful connections, FDDI was reduced significantly in HET animals in peak amplitude (Fig. 6*D*) and in time integral (WT: 0.47 ± 0.09 mV*s; HET: 0.18 ± 0.02 mV*s; $P < 0.01$), as measured at the same resting membrane potential (WT: -58.2 ± 0.6 mV; HET: -59.1 ± 0.6 mV). The latency of the peak response relative to the onset of the presynaptic train showed a trend toward increase that did not reach significance (0.30 ± 0.01 s in WT vs. 0.34 ± 0.02 s in HET; $P = 0.08$). Overall, these results indicate that loss of $Na_V1.1$ channels reduces the reliability of the Martinotti cell-mediated disynaptic inhibitory transmission between neighboring pyramidal neurons. This deficit would greatly disinhibit circuit output from layer V of the neocortex.

Firing of Martinotti cells is highly dependent on the facilitation and summation of presynaptic EPSCs arriving from the pyramidal cell to bring the Martinotti cell to threshold. As a consequence, Martinotti cell firing and the resultant FDDI is a steep function of presynaptic AP frequency and number. Therefore, we tested the dependence of the disynaptic inhibition on the activity of pyramidal neurons by changing the frequency and the number of APs in the presynaptic stimulus train. We first tested the frequency dependence (15 pulses at 20, 30, 50, 70, and 100 Hz) (Fig. 7*A*). Measurable FDDI increases with increased stimulus frequency in both WT and HET, but FDDI was reduced at all frequencies in HET cells relative to WT. We found that, for the successful pairs identified by stimulation at 70 Hz and 100 Hz, the connection probabilities were reduced dramatically in HET cells at lower frequencies (20–50 Hz), consistent with substantial impairment of Martinotti cell firing and resultant disynaptic inhibitory transmission

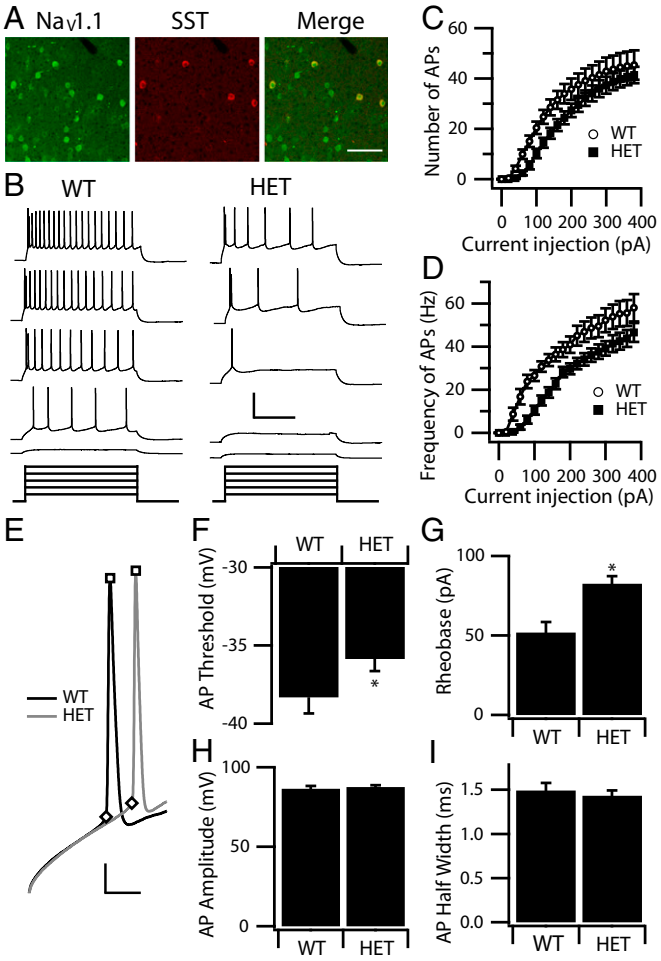

Fig. 4. Excitability of cortical layer V SST interneurons. (*A*) Cortical layer V SST interneurons were double labeled with anti-Na$_V$1.1 (green) and anti-SST antibody (red) to show the presence of anti-Na$_V$1.1 channels in SST interneurons. The merged image shows double-labeled SST interneurons in yellow. (Scale bar: 100 μm.) (*B*) Sample traces of whole-cell current-clamp recordings in response to incremental steps of current (1 s, ranging from 40–200 pA) in a WT and a HET SST interneuron. (Calibration: 0.6 s, 60 mV.) (*C* and *D*) The mean number (*C*) and frequency (*D*) of APs in response to each step for WT ($n = 21$) and HET ($n = 23$). Note that HET SST interneurons require larger current injections to trigger spikes. (*E–I*) Properties of individual WT and HET APs. (*E*) Expanded and superimposed individual APs from recordings of the WT and HET SST interneurons in *B*. (Calibration: 5 ms, 20 mV.) (*F*) Mean AP threshold. (*G*) Mean AP rheobase. (*H*) Mean AP amplitude. (*I*) Mean AP half width. $^*P < 0.05$.

(Fig. 7*B*). Moreover, the amplitude and time integral of the measurable disynaptic responses increased with presynaptic frequency in both WT and HET animals, but HET animals displayed a major defect at all frequencies in both the amplitude (Fig. 7*C*) and time integral (Fig. 7*D*) of the response. The peak latency of the disynaptic response decreased as a function of the frequency of the presynaptic AP train but was similar in WT and HET animals (Fig. 7*E*).

We then examined disynaptic responses after stimulating presynaptic pyramidal neurons with different numbers of APs (5, 8, 10, 12, 15, 20, and 30 pulses) at the same frequency (70 Hz) (Fig. 8*A*). For pairs with disynaptic responses when stimulated with 15 APs at 70 Hz, FDDI probability was reduced dramatically in HET cells when stimulated by smaller numbers of presynaptic APs (5–12 pulses), confirming that the reliability of the disynaptic transmission was substantially impaired in HET cells (Fig. 8*B*). FDDI increased in both amplitude and time integral with increased AP number, but HET animals displayed major defects in both the amplitude and time integral of their responses to each condition (Fig. 8 *C* and *D*). The peak latency of the disynaptic response did not change as more presynaptic APs were discharged and did not differ between WT and HET animals (Fig. 8*E*). Overall, these results demonstrate that the loss of Na$_V$1.1 channels reduces the membrane excitability of layer V Martinotti cells, and this reduction in excitability strongly impairs the reliability and efficacy of Martinotti cell-mediated FDDI between neighboring pyramidal neurons.

Impaired Monosynaptic Transmission Between Layer V Pyramidal Neurons and Martinotti Cells. We carried out complementary dual current-clamp recordings on pairs of neighboring pyramidal neurons and Martinotti cells in layer V (Fig. 9*A*). Stimulation of the pyramidal neuron to elicit a single AP or a small train of APs (Pre PY) elicited postsynaptic responses (Post SST) that increased with AP number (Fig. 9*D*). This excitatory connection is highly facilitating in both WT and HET, consistent with previous studies (27). In response to the same number of presynaptic APs, the postsynaptic response in HET Martinotti cells (shown in gray in Fig. 9*D*) was reduced compared with the postsynaptic response in WT cells (shown in black in Fig. 9*D*). We quantified the amplitudes of postsynaptic EPSPs in Martinotti cells evoked by one, three, and five presynaptic APs, where no postsynaptic APs were elicited, and observed a significant reduction of the excitability in HET as compared with WT Martinotti cells (Fig. 9*B*). The presynaptic pyramidal neurons were stimulated with trains of 1–30 APs at 70 Hz. Facilitating EPSPs were elicited in postsynaptic Martinotti cells, and, when presynaptic AP number increased, summation of EPSCs brought the Martinotti cells to threshold and evoked APs in postsynaptic Martinotti cells after 10–30 APs (Fig. 9*D*, *Lower row*), in agreement with the dependence of FDDI on presynaptic AP numbers (Fig. 8). We quantified the number of postsynaptic APs evoked by presynaptic stimulation and found that postsynaptic HET Martinotti cells were dramatically impaired in the ability to fire APs in response to presynaptic volleys of the same number of APs (Fig. 9*C*).

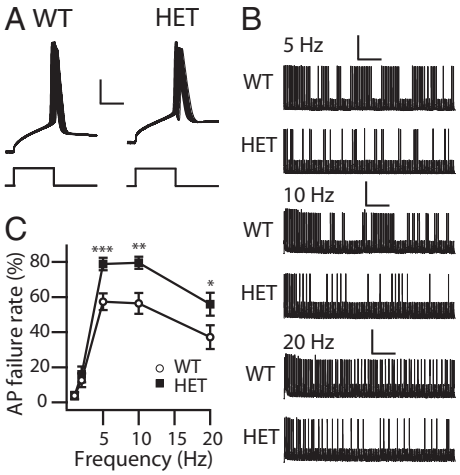

Fig. 5. Ability of cortical layer V SST interneurons to sustain repetitive firing. Whole-cell current-clamp recordings in response to trains of 100 10-ms pulses. Pulse amplitude was the minimum current to trigger an AP. Frequency was 1, 2, 5, 10, or 20 Hz. (*A*) Sample APs of the 1-Hz train for WT and HET SST interneurons. (Calibration: 4 ms, 25 mV.) (*B*) Sample traces at 5 (calibration: 2 s, 40 mV), 10 (calibration: 1 s, 40 mV), and 20 (calibration: 0.5 s, 40 mV) Hz. (*C*) Percent of stimuli that failed to produce an AP as a function of frequency. $^*P < 0.05$; $^{**}P < 0.01$; $^{***}P < 0.001$.

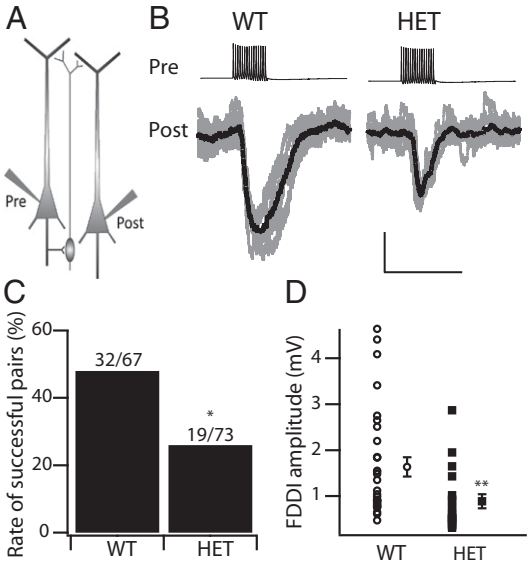

Fig. 6. Martinotti cell-mediated FDDI. (*A*) Cartoon showing the dual patch clamp of a pair of neighboring layer V pyramidal neurons with an intermediate layer V Martinotti cell. (*B*) A train of 15 APs at 70 Hz in one pyramidal neuron (*Upper*) triggered a delayed hyperpolarization (*Lower*) in the second pyramidal neuron. Ten representative traces (gray) and their average (black) are superimposed. (Calibration: 0.2 s, 0.5 mV.) (*C*) Fraction of dual patch-clamp recordings producing measurable disynaptic inhibition using this protocol. WT: 48%, 32/67; HET: 26%, 19/73; Fisher's exact test, $*P = 0.009$. (*D*) Amplitude of disynaptic inhibition in successful pairs. WT: 1.63 ± 0.22 mV ($n = 35$), HET: 0.89 ± 0.15 mV ($n = 19$); $**P = 0.0035$.

These data indicate that reduction in excitability of postsynaptic Martinotti cells underlies the impairment of reliability and efficacy of Martinotti cell-mediated FDDI between neighboring pyramidal neurons observed in the experiments of Figs. 6–8.

We also examined the inhibitory monosynaptic connection from layer V Martinotti cells to pyramidal neurons (Fig. 9 *E* and *F*). Stimulation of Martinotti cells to generate trains of 1–20 presynaptic APs at 70 Hz reliably elicited postsynaptic responses whose size increased with AP number (Fig. 9*F*). We quantified the amplitudes of the inhibitory postsynaptic potentials (IPSPs) in pyramidal neurons and did not observe any significant differences between WT and HET Martinotti cells (Fig. 9*E*). Thus, the ability of the pyramidal neurons to respond to inhibitory synaptic input from Martinotti cells was not impaired when cells were stimulated strongly enough to generate the same number of presynaptic APs in Martinotti cells from WT and DS mice. These results are consistent with impaired excitability of Martinotti cells in DS mice without any adverse effects on Layer V pyramidal cells.

Lack of Effect of $Na_V1.1$ Deletion on Excitability of Layer V Pyramidal Cells. To test further whether the loss of $Na_V1.1$ channels in pyramidal neurons affects their excitability and contributes to the impairment of Martinotti cell-mediated disynaptic inhibition, we compared the electrophysiological properties of layer V pyramidal neurons from WT and HET animals. We did not observe any changes in their input resistance, membrane capacitance, or resting membrane potential (Table 1). In response to incremental steps of current injection (1 s) (Fig. S3*A*), WT and HET pyramidal neurons fired similar numbers of APs (Fig. S3*B*) at similar frequencies (Fig. S3*C*). We also measured the single AP properties of pyramidal neurons from both WT and HET animals (Fig. S3*D*) and found no difference in their spike threshold (Fig. S3*E*), spike amplitude (Fig. S3*F*), rheobase (Fig. S3*G*), or spike width (Fig. S3*H*). Thus, heterozygous deletion of $Na_V1.1$ channels does not change the excitability of cortical layer V pyramidal neurons. These data also confirmed that the impairment of Martinotti cell-mediated disynaptic inhibition (Figs. 6–8) resulted from the reduced excitability of Martinotti cells, as shown in Figs. 4 and 5, and was not influenced by changes in the excitability of the layer V pyramidal neurons.

Discussion

Impairment of the excitability of interneurons in the forebrain is known to cause hyperexcitability, epilepsy, and comorbidities in DS mice (8, 9, 13, 15, 37, 38), but it has remained unclear which types of interneurons in the neocortex contribute to the epileptogenesis and behavioral phenotypes in this devastating disease. Here we report that *Scn1a* haploinsufficiency causes substantial reduction in the membrane excitability of both fast-spiking PV-expressing interneurons and SST-expressing interneurons in a mouse model of DS. In addition, there is a large reduction in FDDI between neighboring pyramidal neurons in layer V of the neocortex mediated by SST-expressing Martinotti cells. Our results

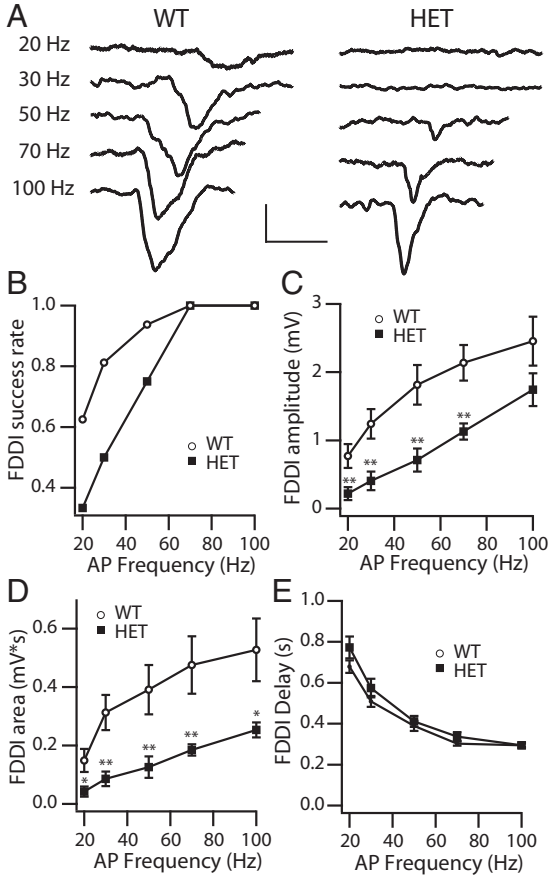

Fig. 7. Frequency dependence of FDDI. (*A*) Examples of traces of FDDI in response to 15 presynaptic APs at the indicated frequencies. (Calibration: 0.2 s, 1 mV.) (*B*) Fraction of recordings giving measurable FDDI at lower frequency for pairs with measurable Martinotti cell-mediated FDDI in response to 15 presynaptic APs at 70 Hz and 100 Hz. (*C* and *D*) Peak FDDI amplitude (*C*) and area (*D*) as a function of frequency. Fifteen presynaptic APs were generated at the indicated frequencies (WT, $n = 16$; HET, $n = 12$) $*P < 0.05$; $**P < 0.01$. (*E*) The peak latency of the Martinotti cell-mediated FDDI decreases as a function of the frequency of the presynaptic AP train in both WT and HET animals at 20 Hz (0.68 ± 0.03 ms in WT vs. 0.77 ± 0.05 ms in HET; $P = 0.17$), 30 Hz (0.51 ± 0.03 ms in WT vs. 0.57 ± 0.05 ms in HET; $P = 0.17$), 50 Hz (0.39 ± 0.03 ms in WT vs. 0.41 ± 0.03 ms in HET; $P = 0.31$), 70 Hz (0.30 ± 0.01 ms in WT vs. 0.34 ± 0.02 ms in HET; $P = 0.09$), and 100 Hz (0.29 ± 0.01 ms in WT vs. 0.29 ± 0.01 ms in HET; $P = 0.48$).

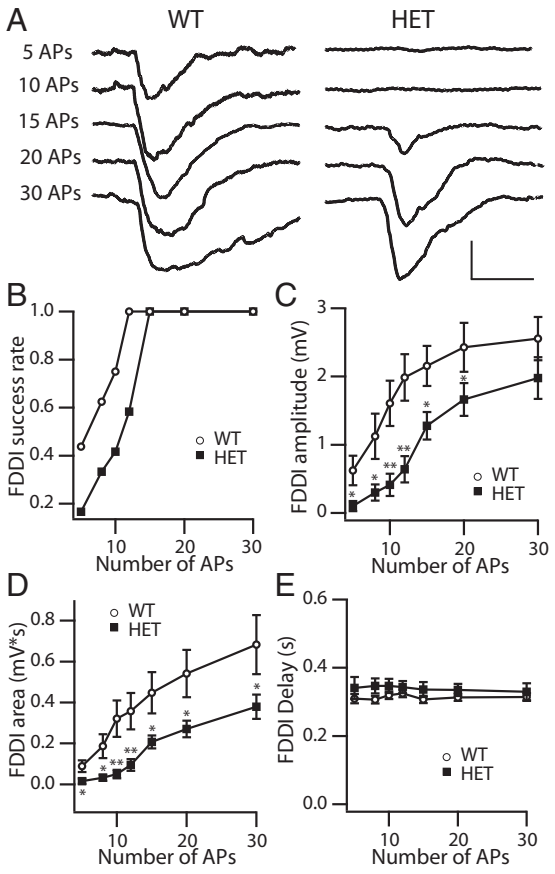

Fig. 8. Dependence of FDDI on the number of presynaptic APs. (*A*) Examples of FDDI in response to 5, 10, 15, 20, and 30 presynaptic APs at 70 Hz. (Calibration: 0.2 s, 1 mV.) (*B*) Fraction of recordings giving measurable FDDI in response to fewer stimuli for pairs with measurable Martinotti cell-mediated FDDI in response to 15 presynaptic APs at 70 Hz. (*C* and *D*) Peak FDDI amplitude (*C*) and area (*D*) as a function of number of presynaptic APs (WT, $n = 16$; HET, $n = 12$). (*E*) The peak latency of the Martinotti cell-mediated FDDI did not change in response to presynaptic stimulation with five APs (0.31 ± 0.01 ms in WT vs. 0.34 ± 0.03 ms in HET; $P = 0.38$), eight APs (0.31 ± 0.01 ms in WT vs. 0.35 ± 0.02 ms in HET; $P = 0.16$), 10 APs (0.32 ± 0.01 ms in WT vs. 0.34 ± 0.02 ms in HET; $P = 0.25$), 12 APs (0.31 ± 0.01 ms in WT vs. 0.34 ± 0.02 ms in HET; $P = 0.13$), 15 APs (0.31 ± 0.01 ms in WT vs. 0.34 ± 0.03 ms in HET; $P = 0.38$), 20 APs (0.31 ± 0.01 ms in WT vs. 0.34 ± 0.02 ms in HET; $P = 0.14$), or 30 APs (0.31 ± 0.01 ms in WT vs. 0.33 ± 0.03 ms in HET; $P = 0.29$).

give crucial insights into the functional deficits of different subtypes of neocortical interneurons in DS and show that circuit output from layer V would be disinhibited dramatically by multiple complementary deficits in interneuron function.

Sodium Currents in Cell Bodies of Cortical GABAergic-Inhibitory Interneurons. $Na_V1.1$ channels are expressed throughout the brain in cell bodies and axon initial segments of both pyramidal neurons and interneurons (8, 9, 30, 31, 39, 40). Therefore, it is surprising that the results from dissociated cells revealed no detectable change in the amplitude, kinetics, or voltage dependence of sodium currents recorded from the cell bodies of cortical interneurons. These results contrast with dissociated inhibitory neurons from hippocampus and cerebellum, in which a substantial reduction in cell body sodium currents was observed (8, 10). $Na_V1.1$ channels may comprise only a minority of sodium channels in the cell bodies of layer V cortical interneurons as a whole, or other sodium channels may be up-regulated in the cell body to compensate for the reduction in activity of $Na_V1.1$ channels in this mixed dissociated cell population. Because of the great diversity of cortical interneurons, it is also possible that different expression levels of sodium channel subtypes in the cell bodies of different classes of interneurons might make changes in $Na_V1.1$ channel expression in specific classes of interneurons undetectable in the entire population of dissociated interneurons.

Excitability of PV Interneurons Is Impaired in DS Mice. Our results show that PV interneurons in layer V have an increased threshold and rheobase for AP generation and decreased amplitude of APs. These deficits combine to reduce the number and frequency of APs fired in response to steady depolarizing stimuli, and they dramatically increase the rate of failure of AP generation in trains of stimuli. Because PV interneurons inhibit their postsynaptic pyramidal cell partners by generating long trains of APs (17, 41), these deficits would cause substantial disinhibition of pyramidal cell excitability and increase the balance of excitatory to inhibitory neurotransmission in neocortical circuits, as we have observed in our recordings of spontaneous cortical synaptic activity (13). Reduced excitability of fast-spiking PV interneurons has been reported to be involved in the generation of seizures in epilepsy and other neurological diseases, such as Alzheimer's disease, autism, and fragile X syndrome (9, 42–45). Because fast-spiking PV interneurons provide strong and direct inhibition to pyramidal neurons, reduced excitability of these cells would be expected to disinhibit the overall network, and restoration of the excitability of these cells has been effective in therapy of these diseases (42, 44). Based on these precedents, it is likely that impaired electrical excitability and AP firing in layer V PV interneurons are major contributors to hyperexcitability, epilepsy, cognitive deficit, and autistic-like behaviors in DS mice.

Excitability of SST Interneurons Is Impaired in DS Mice. Our results show that SST-expressing interneurons also have increased threshold and rheobase for AP generation. These deficits cause a reduced number and frequency of APs in response to steady depolarizing stimuli and an increased failure rate of AP generation in response to trains of stimuli in the critical frequency range of 5–20 Hz. The functional roles of SST interneurons in epilepsy and other neurological diseases are complex and less well-established than for PV interneurons. Reduction in excitability in both SST interneurons and PV interneurons is observed in a rat model of cortical dysplasia (46). Mice lacking the transcription factor Dlx1 display subtype-specific reduction of excitability in cortical SST interneurons and calretinin-expressing interneurons, but not in PV interneurons, and these mice showed generalized electrographic seizures (47). These data suggest that cortical SST interneurons also might be involved in the pathophysiology of epilepsy. Based on these precedents, it is likely that the impaired excitability of SST interneurons we have observed is also an important contributor to the epilepsy and comorbidities of DS.

Site of Impaired AP Generation. In contrast to the unchanged sodium currents in cell bodies of dissociated interneurons, we found substantial deficits in AP firing in intact interneurons in cortical slices. The deficits in threshold and rheobase that we have observed in situ in interneurons in cortical slices would depend primarily on the sodium channels in the axon initial segment, where APs are initiated. Therefore, our results suggest that $Na_V1.1$ channels are important in AP initiation in the axon initial segment of cortical interneurons, and this functional role is not well compensated by up-regulation of other sodium channel types. Previous studies of layer II/III interneurons in a different strain of DS mice led to similar conclusions (9).

Disynaptic Inhibition Mediated by Martinotti Cells Is Impaired in DS Mice. Silberberg and Markram (27) first reported Martinotti cell-mediated FDDI between layer V pyramidal neurons in the

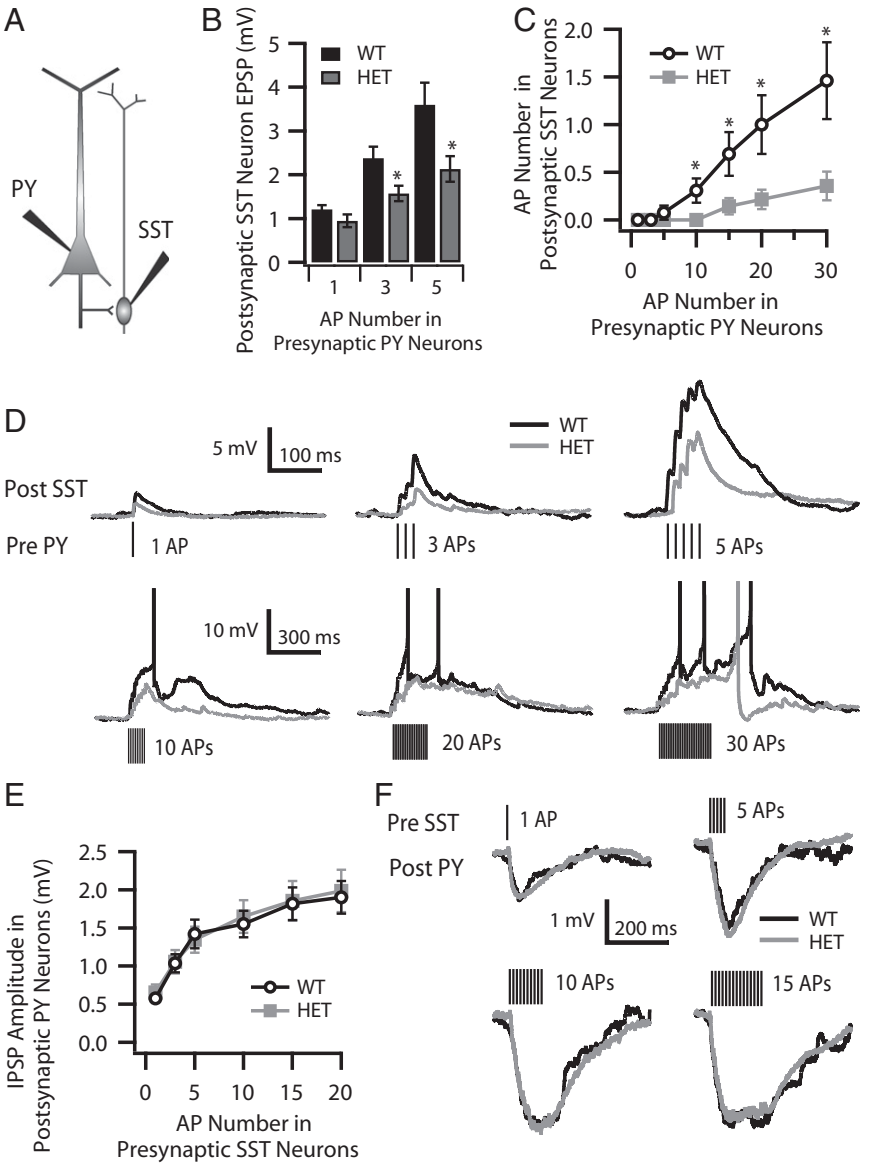

Fig. 9. Monosynaptic connection between layer V pyramidal neurons and Martinotti cells. (*A*) Cartoon showing the dual patch clamp of a layer V pyramidal neuron (PY) and a neighboring layer V Martinotti cell (SST). (*B–D*) Excitatory monosynaptic connection from layer V pyramidal neurons to Martinotti cells. (*B*) The amplitudes of postsynaptic EPSPs in Martinotti cells were reduced in HET compared with WT cells when evoked by one (1.21 ± 0.09 mV in WT vs. 0.95 ± 0.14 mV in HET cells; $P = 0.06$), three (2.38 ± 0.26 mV in WT vs. 1.57 ± 0.18 mV in HET cells; $^*P = 0.01$), and five (3.60 ± 0.50 mV in WT vs. 2.13 ± 0.29 mV in HET cells; $^*P = 0.01$) APs in presynaptic pyramidal neurons. (*C*) The number of postsynaptic APs in Martinotti cells evoked by presynaptic stimulations was impaired dramatically in HET as compared with WT cells when evoked by 10 (0.31 ± 0.13 mV in WT vs. 0 ± 0 mV in HET cells; $^*P = 0.02$), 15 (0.69 ± 0.23 mV in WT vs. 0.13 ± 0.09 mV in HET cells; $^*P = 0.02$), 20 (1.00 ± 0.31 mV in WT vs. 0.21 ± 0.10 mV in HET cells; $^*P = 0.02$), and 30 (1.46 ± 0.36 mV in WT vs. 0.36 ± 0.15 mV in HET; $^*P = 0.01$) APs in presynaptic pyramidal neurons. (*D*) Sample traces (black for WT, gray for HET cells) of EPSPs and evoked APs in Martinotti cells in response to different numbers of APs in presynaptic pyramidal neurons. (*E* and *F*) Inhibitory monosynaptic connection from layer V Martinotti cells to pyramidal neurons. (*E*) The amplitudes of postsynaptic IPSPs in layer V pyramidal neurons as a function of number of presynaptic APs in Martinotti cells. (*F*) Sample traces (black for WT, gray for HET cells) of Martinotti cell-induced postsynaptic IPSPs in layer V pyramidal neurons in response to different numbers of APs in presynaptic pyramidal neurons.

cerebral cortex, and this important inhibitory mechanism has been verified in subsequent studies (28, 48, 49). This disynaptic connection is dynamic, activity-dependent, and strongly facilitating (28). It has been hypothesized that this powerful inhibitory mechanism is important in impeding the spread of hyperactivation of cortical pyramidal neurons and preventing epilepsy (27, 29). Our experiments are fully consistent with this idea, because we have found that FDDI is strikingly impaired in our mouse model of DS. These results provide direct evidence that the reduction of FDDI indeed might contribute to the mechanisms of epileptogenesis and other phenotypes in DS and in epilepsy more broadly.

Excitability of Pyramidal Cells Is Not Impaired in DS Mice. We observed impairment in the excitability of PV interneurons and SST interneurons, whereas the function of the excitatory pyramidal cells in layer V of the neocortex remained unchanged in DS mice. These results indicate that the ratio of excitation to inhibition is increased in layer V neocortical circuits, which are the primary output pathway of the neocortex. The hyperexcitability of these circuits is expected to contribute in an important way to initiation and propagation of epileptic seizures.

In contrast to our results in mice, studies of human induced pluripotent stem cells have given mixed results with respect to effects on excitatory vs. inhibitory neurons (50, 51). One study of

human pluripotent stem cells induced to form cortical neurons in culture reported that the excitability of both pyramidal neurons and bipolar interneurons was paradoxically increased by heterozygous loss-of-function mutations in $Na_V1.1$ channels (50). Another study of human pluripotent stem cells induced to form cortical neurons reported functional decline in the excitability in DS neurons, especially in cortical interneurons (51). These contrasting results illustrate the uncertainties of interpretation of data from these immature culture systems. It is likely that this apparent discrepancy compared with our results with cortical neurons in situ derives from the immature status of these cultured neurons. Sodium current density in these entire neurons, including axons and dendrites in the voltage-clamp preparation (50), is less than 10% of the level of sodium current that we observe in the dissociated cell bodies of mouse hippocampal and neocortical neurons (Fig. S1 and ref. 8). Under the conditions of cell culture used (52), functional synapses are not formed, the ratio of excitatory to inhibitory neurons is much less than in the postnatal brain, and the layered structure and specific synaptic connections of the cerebral cortex are not formed. It will be interesting to follow the maturation of the human pluripotent stem cells as conditions that induce adult neuronal differentiation improve and to compare their properties further with those of mature neurons in brain slices.

Synergistic Actions of PV and SST Interneurons in Controlling Neocortical Excitability. Neocortical interneurons display great diversity in their morphological, physiological, molecular, and synaptic characteristics (16, 17). Two major subgroups of interneurons (fast-spiking PV interneurons and SST-expressing Martinotti cells) comprise more than 80% of the total population of interneurons in layer V of the cortex and are considered the major regulators of the excitability of the pyramidal neurons (17). PV interneurons control the vertical spread of excitability in cortical layers, whereas Martinotti cells control the horizontal spread (16, 17, 53). These complementary actions provide versatile and powerful control of the excitability of neocortical circuits. Therefore, the major deficits in electrical excitability of these two classes of interneurons that we have observed in DS mice would work synergistically to impair inhibitory control of neocortical function and also might lead to neurodevelopmental changes that contribute to the phenotypes of DS. It is likely that this dual impairment of excitability and repetitive AP firing of PV-expressing interneurons and SST-expressing Martinotti cells in layer V of the neocortex contributes substantially to the pathophysiology of DS, including hyperexcitability, epilepsy, cognitive deficit, and autistic-like behaviors.

Materials and Methods

Mouse Strains. *Scn1a* mutant mice were generated by targeted deletion of the last exon encoding domain IV from the S3–S6 segments and the entire C-terminal tail of $Na_V1.1$ channels as described previously (8). Mutant mice were generated on a congenic 129/SvJ background and backcrossed to a C57BL/6J background for at least 10 generations. Animals for this study were generated by crossing heterozygous mutant males of C57BL/6J background with WT C57BL/6J females, or vice versa; from this cross WT and HET mice were born in a 1:1 ratio. Mice were genotyped using a four-oligonucleotide multiplex PCR of genomic DNA samples isolated from mouse tails (54), as described previously (8, 10). To facilitate identification of fast-spiking PV interneurons in the cerebral cortex, we crossed $Na_V1.1$ HET mice with heterozygous G42 GAD67-GFP mice ($Gad1^{EGFP/+}$; Jackson Laboratory), which selectively express eGFP in the PV-expressing subclass of cortical basket cell interneurons in a C57BL/6J/CB6F1 background, to obtain $Gad1^{EGFP/+}$:*Scn*1a$^{+/+}$ and $Gad1^{EGFP/+}$:$Scn1a^{+/-}$ mice (9, 55, 56). All experiments were performed according to guidelines established in the National Institutes of Health *Guide for the Care and Use of Laboratory Animals* (57) and were approved by the University of Washington Institutional Animal Care and Use Committee.

Brain Slice Preparation. Somatosensory cortical brain slices were prepared from P20–P22 mice using standard procedures modified from those previously described (58). Briefly, mice were deeply anesthetized with isoflurane and were decapitated. The brain was removed quickly, and coronal brain slices of frontal cerebral cortex (400 μm) were cut with a modified Vibratome (Pelco 101 series 1000; Ted Pella, Inc.) in chilled (0–4 °C) slicing solution containing 75 mM sucrose, 87 mM NaCl, 25 mM $NaHCO_3$, 25 mM D-glucose, 2.5 mM KCl, 1.25 mM NaH_2PO_4, 0.5 mM $CaCl_2$, 7.0 mM $MgCl_2$, pH 7.3. The slices were transferred to a storage chamber with fresh artificial cerebrospinal fluid (aCSF) containing 126 mM NaCl, 2.5 mM KCl, 2.0 mM $MgCl_2$, 2.0 mM $CaCl_2$, 1.25 mM NaH_2PO_4, 26 mM $NaHCO_3$, and 10 mM D-glucose, pH 7.3, and were incubated at 37 °C for 45 min. The slices then were incubated at room temperature for at least another 45 min before recording. All solutions were saturated with 95% O_2 and 5% CO_2.

Electrophysiological Recordings of Acutely Dissociated Cortical Neurons. The electrophysiological recording of acutely dissociated cortical neurons is described in *SI Materials and Methods*.

Electrophysiological Recordings in Brain Slices. Whole-cell current-clamp recordings from cortical layer V pyramidal cells and interneurons were performed in slices of $Gad1^{EGFP/+}$:$Scn1a^{+/+}$ and $Gad1^{EGFP/+}$:$Scn1a^{+/-}$ mice at room temperature (22–24 °C). Individual slices were transferred to a recording chamber located on an upright microscope (BX51WI; Olympus) and were perfused with oxygenated aCSF (2 mL/min). Neurons were visualized using IR-differential interference contrast microscopy. Layer V pyramidal cells were easily distinguished from interneurons by their triangular morphology, large soma, and pronounced apical dendrite. PV-expressing interneurons were recognized as $eGFP^+$ cells in layer V using fluorescence. All recorded $eGFP^+$ PV interneurons displayed typical fast-spiking patterns. SST-expressing Martinotti cells were selected from $eGFP^-$ interneurons in layer V by their typical ovoid-shaped somata and were finally confirmed by electrophysiological recordings as displaying spike frequency accommodation and burst onset in response to somatic step current injections (27, 33). Patch electrodes were pulled from 1.5-mm o.d. thin-walled glass capillaries (150F-4; World Precision Instruments;) in three stages on a Flaming–Brown micropipette puller (model P-97; Sutter Instruments) and were filled with intracellular solution containing (in mM): 140 K-gluconate, 10 Hepes, 1.1 EGTA, 0.1 $CaCl_2$, 4 Mg-ATP, and 0.5 Na-GTP, pH 7.2. When patch electrodes were filled with intracellular solution, their resistance ranged from 3–5 MΩ. Recordings were obtained through a double patch-clamp EPC 10 system (HEKA) under control of Patchmaster (HEKA). Access resistance was monitored continuously for each cell. Only cells with access resistance less than 20 MΩ were recorded, and recordings were terminated/discarded when a significant (>10%) increase in access resistance occurred.

Analysis of Electrophysiological Results. Data from electrophysiology experiments were analyzed using Igor Pro-6.0 (Wavemetrics). The following parameters were measured to characterize neuronal membrane properties: resting membrane potential (E_m) was recorded immediately after the rupture of the neuronal membrane; input resistance (R_{in}) was determined by measuring the voltage change in response to a small hyperpolarizing current pulse (−40 pA, 1 s) at E_m; membrane capacitance (C_m) was determined by a mono-exponential fit to the voltage produced by a small hyperpolarizing current pulse (−40 pA, 1 s) at resting potential; rheobase was defined as the smallest rectangular current injection that elicited an AP; AP threshold was defined as the membrane potential at the point at which derivatives of voltage with respect to time = 10 mV/ms; AP amplitude was measured between threshold and AP peak; AP width was measured at half height between threshold and AP peak; the AP frequency adaptation ratio was defined as the ratio between the steady-state frequency (the reciprocal of the average of the last four interspike intervals) and the initial frequency (the reciprocal of the first four interspike intervals); the AP amplitude adaptation ratio was defined as the ratio of the steady-state amplitude (the average of the last four AP amplitudes) to the initial amplitude (the average of the first four AP amplitudes); protocols were adapted from ref. 25. Population data are presented as mean ± SEM. Mean values of different groups were compared using Student *t* test. Statistical significance was defined as $P < 0.05$. *P* values in figures are $*P < 0.05$; $**P < 0.01$; $***P < 0.001$.

Immunohistochemistry. P21 mice were anesthetized and perfused intracardially with 4% paraformaldehyde. The brains were removed and cryoprotected by immersion in 10% (wt/vol) sucrose in phosphate buffer (0.1 M Na_2P0_4, pH 7) followed by 30% (wt/vol) sucrose. Brains were sliced (50 μm)

and processed for immunocytochemistry as described previously (8). Briefly, the tissue was rinsed and then incubated in anti-Nav1.1 (1:100) (15) and anti-SST (1:100; Pierce) or anti-PV (1:500; Abcam) for 36 h at 4 °C and then was rinsed again. For double labeling, anti-Nav1.1 was detected using biotinylated goat anti-rabbit IgG (1:300; Vector) and avidin D fluorescein (1:300; Vector). Anti-SST or anti-PV was detected using anti-mouse IgG Alexa 555 (1:1,000; Invitrogen). Sections were rinsed, mounted, coverslipped, and then viewed using a Leica SL confocal microscope in the W. M. Keck Imaging Center at the University of Washington, Seattle, WA. For controls, the primary antiserum was omitted or replaced with normal rabbit serum. No specific labeling was observed in controls.

ACKNOWLEDGMENTS. We thank Dr. Felix Viana (Instituto de Neurosciencas, Universidad Miguel Hernandez) for early brain slice recordings that contributed to the foundation for this work. This research was supported by National Institutes of Health Research Grant R01 NS25704 (to W.A.C.).

1. Wolff M, Cassé-Perrot C, Dravet C (2006) Severe myoclonic epilepsy of infants (Dravet syndrome): Natural history and neuropsychological findings. *Epilepsia* 47(Suppl 2): 45–48.
2. Genton P, Velizarova R, Dravet C (2011) Dravet syndrome: The long-term outcome. *Epilepsia* 52(Suppl 2):44–49.
3. Brunklaus A, Dorris L, Zuberi SM (2011) Comorbidities and predictors of health-related quality of life in Dravet syndrome. *Epilepsia* 52(8):1476–1482.
4. Claes L, et al. (2001) De novo mutations in the sodium-channel gene SCN1A cause severe myoclonic epilepsy of infancy. *Am J Hum Genet* 68(6):1327–1332.
5. Claes LR, et al. (2009) The SCN1A variant database: A novel research and diagnostic tool. *Hum Mutat* 30(10):E904–E920.
6. Rilstone JJ, Coelho FM, Minassian BA, Andrade DM (2012) Dravet syndrome: Seizure control and gait in adults with different SCN1A mutations. *Epilepsia* 53(8):1421–1428.
7. Akiyama M, Kobayashi K, Ohtsuka Y (2012) Dravet syndrome: A genetic epileptic disorder. *Acta Med Okayama* 66(5):369–376.
8. Yu FH, et al. (2006) Reduced sodium current in GABAergic interneurons in a mouse model of severe myoclonic epilepsy in infancy. *Nat Neurosci* 9(9):1142–1149.
9. Ogiwara I, et al. (2007) Nav1.1 localizes to axons of parvalbumin-positive inhibitory interneurons: A circuit basis for epileptic seizures in mice carrying an Scn1a gene mutation. *J Neurosci* 27(22):5903–5914.
10. Kalume F, Yu FH, Westenbroek RE, Scheuer T, Catterall WA (2007) Reduced sodium current in Purkinje neurons from Nav1.1 mutant mice: Implications for ataxia in severe myoclonic epilepsy in infancy. *J Neurosci* 27(41):11065–11074.
11. Oakley JC, Kalume F, Yu FH, Scheuer T, Catterall WA (2009) Temperature- and age-dependent seizures in a mouse model of severe myoclonic epilepsy in infancy. *Proc Natl Acad Sci USA* 106(10):3994–3999.
12. Han S, et al. (2012) $Na_{(v)}1.1$ channels are critical for intercellular communication in the suprachiasmatic nucleus and for normal circadian rhythms. *Proc Natl Acad Sci USA* 109(6):E368–E377.
13. Han S, et al. (2012) Autistic-like behaviour in Scn1a+/- mice and rescue by enhanced GABA-mediated neurotransmission. *Nature* 489(7416):385–390.
14. Kalume F, et al. (2013) Sudden unexpected death in a mouse model of Dravet syndrome. *J Clin Invest* 123(4):1798–1808.
15. Cheah CS, et al. (2012) Specific deletion of $Na_V1.1$ sodium channels in inhibitory interneurons causes seizures and premature death in a mouse model of Dravet syndrome. *Proc Natl Acad Sci USA* 109(36):14646–14651.
16. Markram H, et al. (2004) Interneurons of the neocortical inhibitory system. *Nat Rev Neurosci* 5(10):793–807.
17. Rudy B, Fishell G, Lee S, Hjerling-Leffler J (2011) Three groups of interneurons account for nearly 100% of neocortical GABAergic neurons. *Dev Neurobiol* 71(1):45–61.
18. Ascoli GA, et al.; Petilla Interneuron Nomenclature Group (2008) Petilla terminology: Nomenclature of features of GABAergic interneurons of the cerebral cortex. *Nat Rev Neurosci* 9(7):557–568.
19. Kawaguchi Y, Kubota Y (1997) GABAergic cell subtypes and their synaptic connections in rat frontal cortex. *Cereb Cortex* 7(6):476–486.
20. Xu X, Roby KD, Callaway EM (2010) Immunochemical characterization of inhibitory mouse cortical neurons: Three chemically distinct classes of inhibitory cells. *J Comp Neurol* 518(3):389–404.
21. Hasenstaub A, et al. (2005) Inhibitory postsynaptic potentials carry synchronized frequency information in active cortical networks. *Neuron* 47(3):423–435.
22. Haider B, McCormick DA (2009) Rapid neocortical dynamics: Cellular and network mechanisms. *Neuron* 62(2):171–189.
23. Dutton SB, et al. (2012) Preferential inactivation of Scn1a in parvalbumin interneurons increases seizure susceptibility. *Neurobiol Dis* 49C:211–220.
24. Ogiwara I, et al. (2013) Nav1.1 haploinsufficiency in excitatory neurons ameliorates seizure-associated sudden death in a mouse model of Dravet syndrome. *Hum Mol Genet* 22(23):4784–4804.
25. Xu H, Jeong HY, Tremblay R, Rudy B (2013) Neocortical somatostatin-expressing GABAergic interneurons disinhibit the thalamorecipient layer 4. *Neuron* 77(1):155–167.
26. Ma Y, Hu H, Berrebi AS, Mathers PH, Agmon A (2006) Distinct subtypes of somatostatin-containing neocortical interneurons revealed in transgenic mice. *J Neurosci* 26(19):5069–5082.
27. Silberberg G, Markram H (2007) Disynaptic inhibition between neocortical pyramidal cells mediated by Martinotti cells. *Neuron* 53(5):735–746.
28. Berger TK, Perin R, Silberberg G, Markram H (2009) Frequency-dependent disynaptic inhibition in the pyramidal network: A ubiquitous pathway in the developing rat neocortex. *J Physiol* 587(Pt 22):5411–5425.
29. Murayama M, et al. (2009) Dendritic encoding of sensory stimuli controlled by deep cortical interneurons. *Nature* 457(7233):1137–1141.
30. Duflocq A, Le Bras B, Bullier E, Couraud F, Davenne M (2008) Nav1.1 is predominantly expressed in nodes of Ranvier and axon initial segments. *Mol Cell Neurosci* 39(2): 180–192.
31. Westenbroek RE, Merrick DK, Catterall WA (1989) Differential subcellular localization of the RI and RII Na^+ channel subtypes in central neurons. *Neuron* 3(6):695–704.
32. Goldberg EM, Coulter DA (2013) Mechanisms of epileptogenesis: A convergence on neural circuit dysfunction. *Nat Rev Neurosci* 14(5):337–349.
33. Wang Y, et al. (2004) Anatomical, physiological and molecular properties of Martinotti cells in the somatosensory cortex of the juvenile rat. *J Physiol* 561(Pt 1):65–90.
34. Pignatelli M, Beyeler A, Leinekugel X (2012) Neural circuits underlying the generation of theta oscillations. *J Physiol Paris* 106(3-4):81–92.
35. Benchenane K, Tiesinga PH, Battaglia FP (2011) Oscillations in the prefrontal cortex: A gateway to memory and attention. *Curr Opin Neurobiol* 21(3):475–485.
36. Kapfer C, Glickfeld LL, Atallah BV, Scanziani M (2007) Supralinear increase of recurrent inhibition during sparse activity in the somatosensory cortex. *Nat Neurosci* 10(6):743–753.
37. Martin MS, et al. (2010) Altered function of the SCN1A voltage-gated sodium channel leads to gamma-aminobutyric acid-ergic (GABAergic) interneuron abnormalities. *J Biol Chem* 285(13):9823–9834.
38. Tang B, et al. (2009) A BAC transgenic mouse model reveals neuron subtype-specific effects of a Generalized Epilepsy with Febrile Seizures Plus (GEFS+) mutation. *Neurobiol Dis* 35(1):91–102.
39. Lorincz A, Nusser Z (2008) Cell-type-dependent molecular composition of the axon initial segment. *J Neurosci* 28(53):14329–14340.
40. Vacher H, Mohapatra DP, Trimmer JS (2008) Localization and targeting of voltage-dependent ion channels in mammalian central neurons. *Physiol Rev* 88(4):1407–1447.
41. Bartos M, Elgueta C (2012) Functional characteristics of parvalbumin- and cholecystokinin-expressing basket cells. *J Physiol* 590(Pt 4):669–681.
42. Dölen G, et al. (2007) Correction of fragile X syndrome in mice. *Neuron* 56(6):955–962.
43. Rossignol E (2011) Genetics and function of neocortical GABAergic interneurons in neurodevelopmental disorders. *Neural Plast* 2011:649325.
44. Verret L, et al. (2012) Inhibitory interneuron deficit links altered network activity and cognitive dysfunction in Alzheimer model. *Cell* 149(3):708–721.
45. Rossignol E, Kruglikov I, van den Maagdenberg AM, Rudy B, Fishell G (2013) $Ca_V2.1$ ablation in cortical interneurons selectively impairs fast-spiking basket cells and causes generalized seizures. *Ann Neurol* 74(2):209–222.
46. Zhou FW, Roper SN (2011) Altered firing rates and patterns in interneurons in experimental cortical dysplasia. *Cereb Cortex* 21(7):1645–1658.
47. Cobos I, et al. (2005) Mice lacking Dlx1 show subtype-specific loss of interneurons, reduced inhibition and epilepsy. *Nat Neurosci* 8(8):1059–1068.
48. Buchanan KA, et al. (2012) Target-specific expression of presynaptic NMDA receptors in neocortical microcircuits. *Neuron* 75(3):451–466.
49. Berger TK, Silberberg G, Perin R, Markram H (2010) Brief bursts self-inhibit and correlate the pyramidal network. *PLoS Biol* 8(9):8.
50. Liu Y, et al. (2013) Dravet syndrome patient-derived neurons suggest a novel epilepsy mechanism. *Ann Neurol* 74(1):128–139.
51. Higurashi N, et al. (2013) A human Dravet syndrome model from patient induced pluripotent stem cells. *Mol Brain* 6:19.
52. Banker G, Goslin K (1998) *Culturing Nerve Cells* (Massachusetts Institute of Technology, Boston, MA).
53. DeFelipe J, et al. (2013) New insights into the classification and nomenclature of cortical GABAergic interneurons. *Nat Rev Neurosci* 14(3):202–216.
54. Wu Q, Chen M, Buchwald M, Phillips RA (1995) A simple, rapid method for isolation of high quality genomic DNA from animal tissues. *Nucleic Acids Res* 23(24):5087–5088.
55. Tamamaki N, et al. (2003) Green fluorescent protein expression and colocalization with calretinin, parvalbumin, and somatostatin in the GAD67-GFP knock-in mouse. *J Comp Neurol* 467(1):60–79.
56. Chattopadhyaya B, et al. (2004) Experience and activity-dependent maturation of perisomatic GABAergic innervation in primary visual cortex during a postnatal critical period. *J Neurosci* 24(43):9598–9611.
57. Committee on Care and Use of Laboratory Animals (1985) *Guide for the Care and Use of Laboratory Animals* (Natl Inst Health, Bethesda), DHHS Publ No (NIH) 85-23.
58. Tai C, Kuzmiski JB, MacVicar BA (2006) Muscarinic enhancement of R-type calcium currents in hippocampal CA1 pyramidal neurons. *J Neurosci* 26(23):6249–6258.